PLOS ONE

RESEARCH ARTICLE

Synthesis and optoelectronic properties of Cu_3VSe_4 nanocrystals

Mimi Liu[1], Cheng-Yu Lai[1], Gurpreet Singh Selopal[2,3], Daniela R. Radu[1,4]*

1 Department of Mechanical and Materials Engineering, Florida International University, College of Engineering and Computing, Miami, Florida, United States of America, **2** Institute National de la Recherche Scientifique, Centre Énergie, Matériaux et Télécommunications, Varennes, Québec, Canada, **3** Institute of Fundamental and Frontier Sciences, University of Electronic Science and Technology of China, Chengdu, PR China, **4** Department of Materials Science and Engineering, University of Delaware, Newark, Delaware, United States of America

* dradu@fiu.edu

Citation: Liu M, Lai C-Y, Selopal GS, Radu DR (2020) Synthesis and optoelectronic properties of Cu_3VSe_4 nanocrystals. PLoS ONE 15(5): e0232184. https://doi.org/10.1371/journal.pone.0232184

Editor: P. Davide Cozzoli, University of Salento, ITALY

Received: January 15, 2020

Accepted: April 8, 2020

Published: May 5, 2020

Data Availability Statement: All relevant data are within the paper and its Supporting Information files.

Funding: ML Funding from D.Radu FIU startup funds; DR and CYL National Aeronautics and Space Administration, 80NSSC19M0201, https://www.nasa.gov The funders had no role in study design, data collection and analysis, decision to publish, or preparation of the manuscript CYL National Science Foundation Grant No. 1924412 https://www.nsf.gov The funders had no role in study

Abstract

The ternary chalcogenide Cu_3VSe_4 (CVSe) with sulvanite structure has been theoretically predicted to be a promising candidate for photovoltaic applications due to its suitable band-gap for solar absorption and the relatively earth-abundant elements in its composition. To realize the absorber layer via an inexpensive route, printed thin-films could be fabricated from dispersions of nano-sized Cu_3VSe_4 precursors. Herein, cubic Cu_3VSe_4 nanocrystals were successfully synthesized via a hot-injection method. Similar with reported Cu_3VS_4 nanocrystals, Cu_3VSe_4 nanocrystals with cubic structure exhibit three absorption bands in the UV-Visible range indicative of a potential intermediate bandgap existence. A thin film fabricated by depositing the nanoparticles Cu_3VSe_4 on FTO coated glass substrate, exhibited a p-type behavior and a photocurrent of ~ 4 μA/cm^2 when measured in an electrochemical cell setting. This first demonstration of photocurrent exhibited by a CVSe nanocrystals thin film signifies a promising potential in photovoltaic applications.

Introduction

The class of sulvanites, with the formula Cu_3MCh_4 (M = V, Nb, Ta; Ch = S, Se, Te) is comprised of ternary copper chalcogenide semiconductors with the calculated optical band gap ranging from 1.19 eV to 2.60 eV, theoretically predicted p-type conductivity, and with potential in photovoltaic and optoelectronic applications. [1–3]

As suggested by current thin-film photovoltaic technologies, the absorbing layer of a thin-film solar cell should have an optical band gap of about 1.5 eV and a low hole effective mass. The sulvanites exhibit low hole effective mass of Cu_3MCh_4 decreasing along the chalcogen (Ch = S, Se, Te) series, and increasing with the transition metal group (V, Nb, Ta). [3]

Recently, the Kehoe group reported calculated band gaps of sulvanite structured Cu_3MCh_4. Specifically, the optical band gaps of Cu_3VTe_4, Cu_3NbTe_4, Cu_3VSe_4, Cu_3TaTe_4, and Cu_3VS_4 are 1.19 eV, 1.46 eV, 1.49 eV, 1.69 eV, and 1.72 eV, respectively, are suitable for photovoltaic applications. [3, 4]

design, data collection and analysis, decision to publish, or preparation of the manuscript.

Competing interests: The authors have declared that no competing interests exist.

While the telluride sulvanites Cu_3MTe_4 (M = V, Nb, Ta) present an appealing trend in regard to both their optical bandgap [3] and other applications, materials fabrication seems cumbersome due to the low reactivity and solubility of Te powder in the aliphatic solvents, [5, 6] hindering the wide application of Cu_3MTe_4 (M = V, Nb, Ta) materials. Thus, Cu_3VSe_4 and Cu_3VS_4 remain the sulvanite compounds that present most interest for photovoltaic applications. [7]

Solution-processed inorganic solar cells present a promising low-cost alternative to first-generation solar cells and could lead to technologies compatible with relevant terawatt capacities. [8]

The bottom-up approach for absorber fabrication utilizes nanocrystalline precursors that could be formulated in dispersion amenable to thin film deposition by printing methods. Recently, Chen at. al reported the first sulvanite synthesis in nanocrystalline form—Cu_3VS_4 (CVS) nanocrystals—obtained through a hot-injection synthesis. [9] Subsequently, Mantella et al. demonstrated the ability to control the size of nanocrystals, by synthesized cubic Cu_3VS_4 NCs with different sizes and narrow size distribution. The report also demonstrated the presence of an intermediate bandgap (IB) in Cu_3VS_4 through both theoretical calculations and experimental measurements. [10] Compared with photovoltaic devices with a single bandgap E_g, semiconductors with an intermediate band can reduce the loss of incomplete absorption, since photons with energy below E_g can also be absorbed through transitions from the valence band (VB) to IB or from IB to the conduction band (CB). [11] In addition, because of the multiple-band transitions of VB-IB and IB-CB, the intermediate band semiconductors were proposed to have the possibility to reduce the thermalization effect, compared with single-band semiconductors. [12]

Therefore, it is predicted that semiconductors with intermediate bands have the potential to increase the conversion efficiency of a solar cell as the consequent effect of highly exceeding the Schockley-Queisser limit up to 63.1%. [10, 13] We anticipated that preparation of colloidal Cu_3VSe_4 could be achieved via similar synthetic methodologies.

In this work, we prepared Cu_3VSe_4 nanocrystals (CVSe NCs) by the hot-injection of Se precursor into cations precursor at 260˚C. The obtained CVSe compounds exhibit the crystal structure of bulk CVSe as showed by X-ray diffraction and Raman spectroscopy. The nanocrystals show a cubic shape and particle size of 25 nm according to TEM and SEM analysis. The UV-Vis-NIR spectra of CVSe NCs show three distinct absorption bands that are similar to Cu_3VS_4 NCs. Additionally, the photocurrent of CVSe thin film on FTO substrates evidences its p-type semiconductor nature and great potential in the photovoltaic application.

Materials and methods

Materials

All chemicals used in the experiment were as received without further purification. Vanadium (IV) oxide acetylacetonate ($VO(acac)_2$, $\geq$ 98%) was ordered from Merck KGaA. Selenium powder (Se, 99.99%) and oleylamine (OLA, 70%) were purchased from Aldrich. Copper(I) chloride (CuCl, 99.99%), trioctylphosphine oxide(TOPO, 90%), trioctylphosphine (TOP, 97%) and oleic acid ($\geq$ 99%) were purchased from Sigma-Aldrich. Formamide (FA, 99%) and sodium sulfide (Na_2S, anhydrous) was bought from Alfa Aesar. ACS grade chloroform ($CHCl_3$, $\geq$99.8%), acetone (CH_3OCH_3, $\geq$99.5%), and methanol (CH_3OH, 99.8%) were bought from Fisher Scientific, while ethanol (C_2H_5OH, 100%) was ordered from Decon laboratories. FTO Soda Lime glass substrates were purchased from MSE Supplies.

The crystal structure and purity of prepared CVSe NCs were performed by X-ray diffraction using Siemens Diffractometer D5000 (Cu Kα radiation, λ = 1.5405 Å) and Raman spectra

conducted on the Raman Renishaw microscopy with 633 nm laser. JEOL 6330F Scanning Electron Microscope (SEM) combined with EDS was performed at 25.0 kV accelerating voltage to investigate the elemental distribution of the produced CVSe NCs. Philips CM200 Transmission electron microscopy (TEM) was used to determine the shape and size of the synthesized CVSe NCs. The chemical and electronic structure of the synthesized Cu_3VSe_4 NCs was determined by X-ray photoelectron spectroscopy (XPS) in a VG Escalab 220i-XL equipped with an Al Kα source. Photoluminescence (PL) spectra of CVSe NCs were conducted on PERKIN ELMER LS-55 Luminescence Spectrometer. The absorption spectrum of CVSe NCs was collected using Agilent Cary 5000 UV-vis-NIR spectrophotometer. The thermal stability of the Cu_3VSe_4 nanosheets was determined using a TA Instrument SDT-Q600 Simultaneous TGA/DSC.

Preparation of CVSe NCs

In a typical synthesis, CuCl (1 mmol, 99 mg), vanadium (IV) oxide acetylacetonate (0.7 mmol, 185.5 mg), trioctylphosphine oxide (TOPO, 3 mmol, 1.31g), and 15 mL of oleylamine were loaded to a 100 mL two-neck round bottom flask, followed by degassing at 120˚C for 30 minutes. Meanwhile, the Se source was prepared by dissolving 158 mg selenium powder (2 mmol) in a mixture of 5 mL oleylamine and 3 mL oleic acid and further evacuated at room temperature for 30 minutes. Upon degassing, both vessels were filled with argon. The Cu-V solution was heated to 260˚C, and then the Se precursor was immediately injected at 260˚C. Afterward, the reaction was maintained at 260˚C for 1 hour. First, the product was transferred to the centrifuge tube with 4 mL TOP and ultrasonicated for 5 minutes to remove the residual Se. Then the precipitates were washed two times with a mixture of chloroform and ethanol at a volume ratio of 1:3. The precipitates were collected by centrifugation and dried overnight in a vacuum oven.

Ligand exchange

The organic ligands attached to the surface of the synthesized colloidal nanocrystals are thought to block the charge transport when deposited in films and nanocrystal solids given that the organic ligands may generate insulating layers between the nanocrystals. [14–16]

In this work, a ligand exchange process was conducted to replace the organic ligands coordinated to CVSe NCs during synthesis (oleylamine, oleic acid, TOPO) with inorganic short ligands, S^{2-} by treatment with Na_2S. [15] In a typical experiment, synthesized CVSe were suspended in toluene (8 mg/mL) and an amount of 10 mL of the CVSe suspension was added to a 10 mL of Na_2S formamide solution (0.2 M). Next, the mixture was vigorously shaken for 1 minute and then hold until clear phases separate. The black CVSe NCs were transferred from the toluene phase to the formamide phase, indicating the successful ligand exchange. The clear toluene phase was removed, and a mixture of ethanol and nanopure water (v:v, 4:1) was added to precipitate the Cu_3VSe_4 NCs. The precipitates were washed twice with ethanol and nanopure water (v:v, 4:1), followed by purifying with a mixture of toluene and ethanol (v:v, 1:3). The resulting product was collected by centrifugation and dried in vacuum oven overnight for further use.

Fabrication of CVSe thin film

CVSe dispersions (inks) were prepared by adding 25 mg of ligand exchanged CVSe NCs into 1mL ethanol and dispersed via ultrasonication for 10 minutes. 20 μL CVSe inks was deposited on FTO-coated glass by blade coating, followed by thermal treatment at 100˚C for 1 minute in air, on a hot plate. The deposition process was repeated twice to fabricate the glass/FTO/CVSe

thin film. Prior to deposition, the FTO substrates were cleaned in a sequence of distilled water, methanol, acetone, and ethanol through an ultrasonic bath for 10 minutes, respectively.

Photoelectrochemical measurements

The photoelectrochemical response of CVSe thin film was tested by PINE reseach potentiostat connected with a three-electrode photoelectrochemical cell consisting of an Ag/AgCl reference electrode, a platinum counter electrode and a working electrode of CVSe-coated FTO substrate. All these three electrodes were held in the KCl aqueous solution (0.6 M) with a PH of 4.5. The current-voltage (J-V) curve of the CVSe thin film was swept from 0.6 V to 0 V in steps of 10 seconds light on-off with a sweep rate of 2 mVs^{-1} in the ambient atmosphere. The photocurrent of the CVSe thin film was produced by periodically irradiating LED light with 2000 lumens on the film for 10 seconds and shutting down the light for 10 seconds.

Results and discussion

The CVSe NCs were characterized for crystallinity, purity, stability and composition.

Fig 1A presents the X-ray diffraction of the synthesized CVSe, where each peak can be highly indexed to the cubic CVSe with a space group of $P\bar{4}3m$ (PDF# 40125). Raman spectrum of synthesized CVSe in Fig 1B exhibits five peaks at around 133.4 cm^{-1}, 158.5 cm^{-1}, 185.1 cm^{-1}, 218.3 cm^{-1} and 345.8 cm^{-1}, respectively. The crystal structure of synthesized CVSe is shown in Fig 1C.

The thermal stability of synthesized CVSe NCs was investigated using thermogravimetric analysis (TGA), where 18.5 mg of CVSe NCs were annealed in the range of 25–800˚C at a ramping temperature of 20˚C/min under argon atmosphere. The TGA curve in Fig 1D, conducted from 25˚C to 800˚C, shows two main mass loss events: the first weight loss, which begins at 250˚C, could be associated with the evaporation of the residual organic ligand originated from the solution-phase synthesis, while the second mass loss, around 650˚C correlates

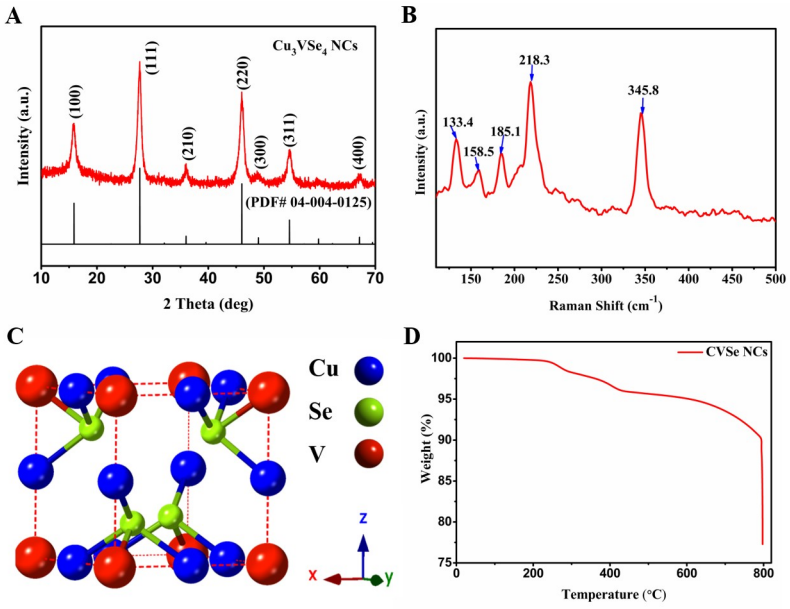

Fig 1. Characterization of CVSe NCs. (A) X-ray diffraction. (B) Raman spectrum. (C) Crystal structure. (D) TGA plot of synthesized CVSe NCs.

https://doi.org/10.1371/journal.pone.0232184.g001

with the decomposition of CVSe NCs. To further understand the stability of CVSe under thermal stress, we annealed CVSe NCs at 650˚C under argon atmosphere for 1 minute and 5 minutes, respectively. As shown in S1 Fig, the XRD pattern of CVSe NCs that was annealed for 1 minute exhibits pure CVSe phase, while the CVSe NCs annealing for 5 minutes displays a mixed phase of $Cu_{1.8}Se$ an CVSe, signifying that CVSe NCs start to decompose at 650˚C.

The low-resolution TEM image in Fig 2A reveals that the as-synthesized CVSe NCs have cubic shape. Fig 2B exhibits the high-resolution TEM (HRTEM) image, showing two measured interplanar spacing (d-spacing) of 0.32 nm and 0.54 nm, corresponding to the (111) plane and (100) of the cubic CVSe, respectively, illustrating the well-crystallized CVSe NCs. The elemental composition of the as-synthesized CVSe NCs was determined by SEM-EDS in Fig 2C–2F, showing a uniform distribution of Cu, V, and Se elements in the selected region. Consistent with XRD and SEM-EDS analysis, the purity of the obtained CVSe was also confirmed by Raman spectroscopy.

X-Ray Photoelectron Spectroscopy (XPS) was performed to determine the oxidation states of elements Cu, V, and Se present in the as-synthesized CVSe NCs. High-resolution XPS spectra of the Cu 2p, V 2p, and Se 3d orbitals are shown in Fig 3. The corresponding Cu $2p_{3/2}$ and Cu $2p_{1/2}$ core-level spectra of CVSe NCs in Fig 3A displays two peaks at 932.4 eV and 952.4 eV, respectively, suggesting that Cu is presented in Cu(I) state. [17–19] Base on the literature, the binding energies of V 2p appear at 516.7 eV(V $2p_{3/2}$) and 523.5 eV (V $2p_{1/2}$) with a separation of 6.8 eV in Fig 3B is close to $V5^+$, [20, 21] whereas, the peaks at 513.5 eV and 521.3 eV with a separation of 7.8 eV corresponded to V $2p_{3/2}$ and V $2p_{1/2}$ in V 2^+. [22–24] However, the XRD data shows only CVSe phase. In the study of Cu_3VS_4 material, Mantella et al. illustrated that the Cu_xS nanoparticles and V-containing nanoparticles (V-NPs) were initially formed during the synthesis of the Cu_3VS_4 NCs. It is worth noting that the XRD of V-NPs showed amorphous status.[10] Thus, we speculated that some amorphous V-NPs could be formed in the synthesized CVSe NCs. The fitted spectrum of Se 3d in Fig 3C presents a peak at 53.8 eV which can be attributed to the Se $3d_{3/2}$ of Se^{2-}. [25–27]

Overall, the XPS results demonstrate that the oxidation states of Cu, V, and Se in Cu_3VSe_4 NCs are the same as in bulk: +1, +5, and -2, respectively.

Fig 4A shows the UV-Vis-NIR spectrum of synthesized CVSe NCs in ethanol, where three broad peaks were identified at around 391 nm, 562 nm, and 678 nm. When converting the

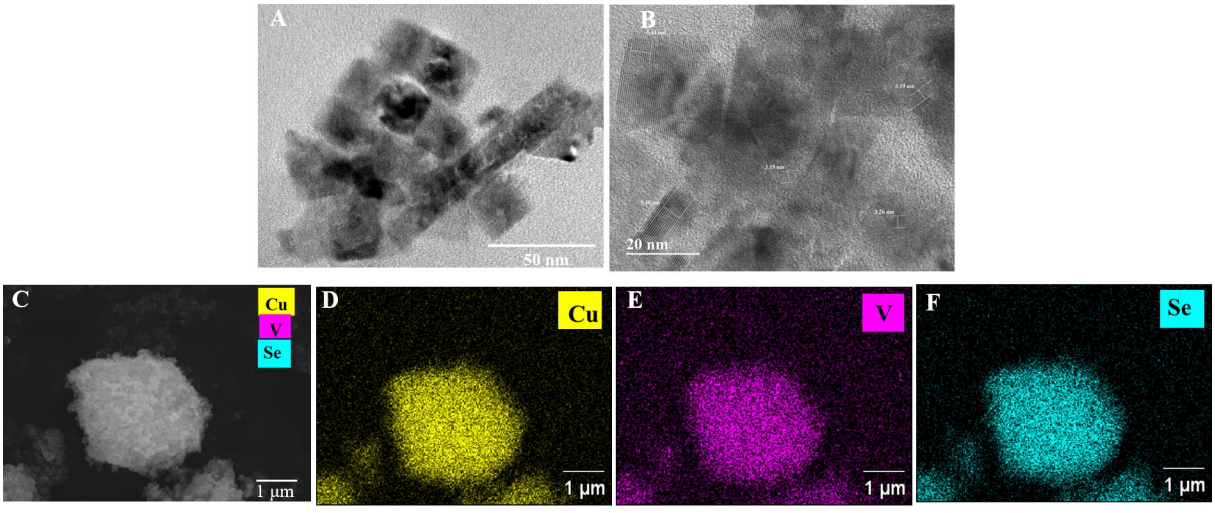

Fig 2. (A) Low-resolution TEM images. (B) HRTEM images. (C) SEM image of synthesized CVSe NCs. (D-F) SEM–EDS elemental mapping of CVSe NCs.

https://doi.org/10.1371/journal.pone.0232184.g002

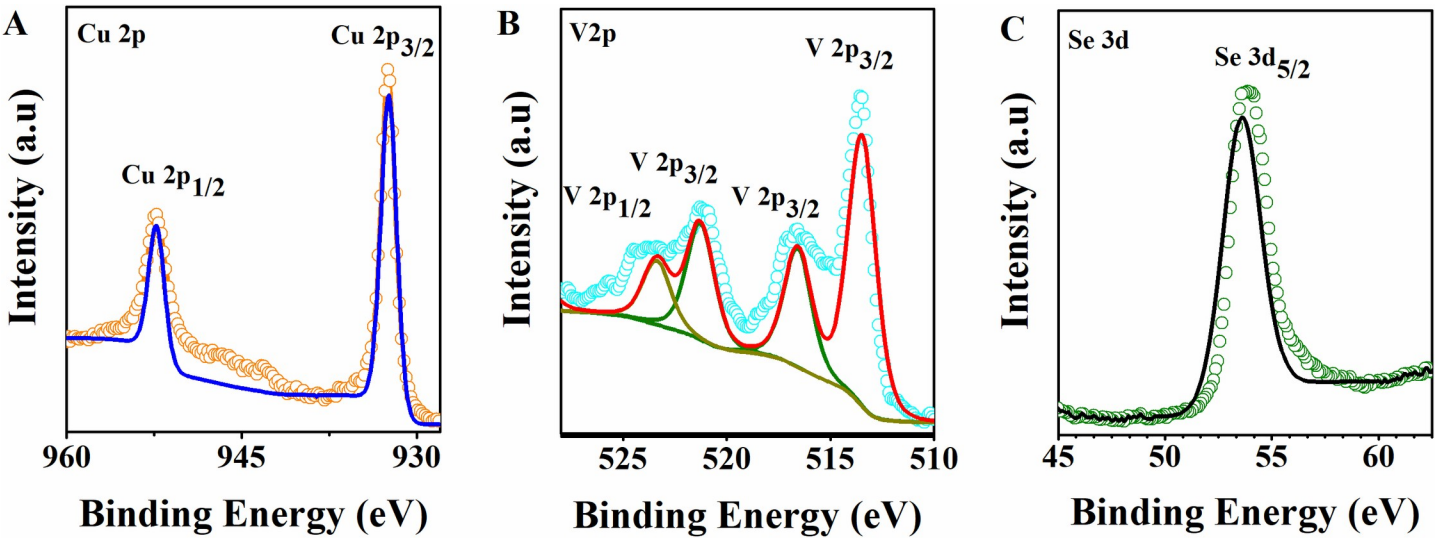

Fig 3. XPS spectra of the Cu 2p, V 2p and Se 3d peaks of CVSe NCs.

https://doi.org/10.1371/journal.pone.0232184.g003

wavelength to photo energy, these three absorption bands correspond to 3.17 eV, 2.20 eV and 1.83 eV which are in accordance with bandgap of VB-CB, VB-IB I, and VB-IB II, respectively. [28, 29]

Thin Film. Mitigation of residual carbon-based ligands on nanoparticles surface is reported as beneficial for thin film fabrication. Therefore, before depositing CVSe NCs inks on the FTO substrate, a ligand exchange process was conducted to remove the organic ligands, and their removal confirmed by infrared spectroscopy. Fig 4B displays the FTIR spectra of the as-synthesized CVSe NCs (blue line) and the NCs with ligand exchange (red line). The CVSe NCs were synthesized in the presence of oleylamine, oleic acid, and TOPO as solvent or surfactant. Thus, the characteristic band at around 1465 cm^{-1} corresponds to the P-C bond vibrational stretching; the characteristic doublet at around 2852 and 2925 cm^{-1} could be attributed to C-H stretching mode, suggesting that the synthesized CVSe NCs are capped with TOPO. These organic ligand-capped synthetic CVSe NCs underwent a ligand exchange with Na_2S-formamide solution, and then the CVSe NCs transferred from chloroform to the formamide phase to generate inorganic ligand S^{2-}terminated CVSe NCs, as shown in **Fig 4B** red line, where the C-H and C-P stretching apparently disappeared. The XRD pattern and Raman spectrum of the product after ligand exchange show pure CVSe phase, as shown in **S2 Fig** and **S3 Fig**.

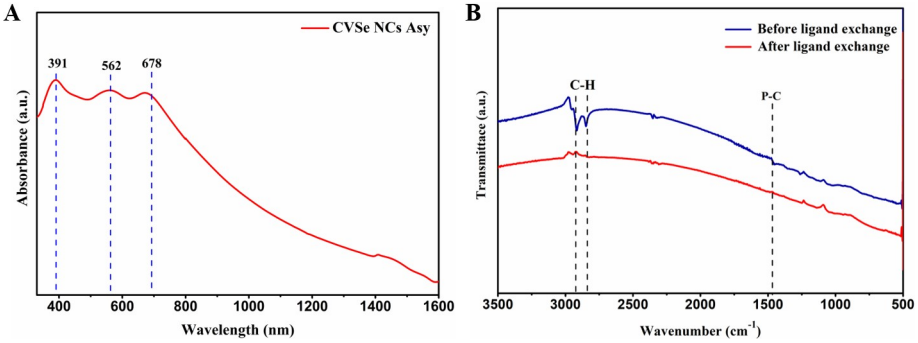

Fig 4. (A) UV-Vis-NIR spectra of the synthesized CVSe NCs in ethanol (B) FTIR spectra of the as-synthesized CVSe NCs (blue line) and CVSe with ligand exchange (red line).

https://doi.org/10.1371/journal.pone.0232184.g004

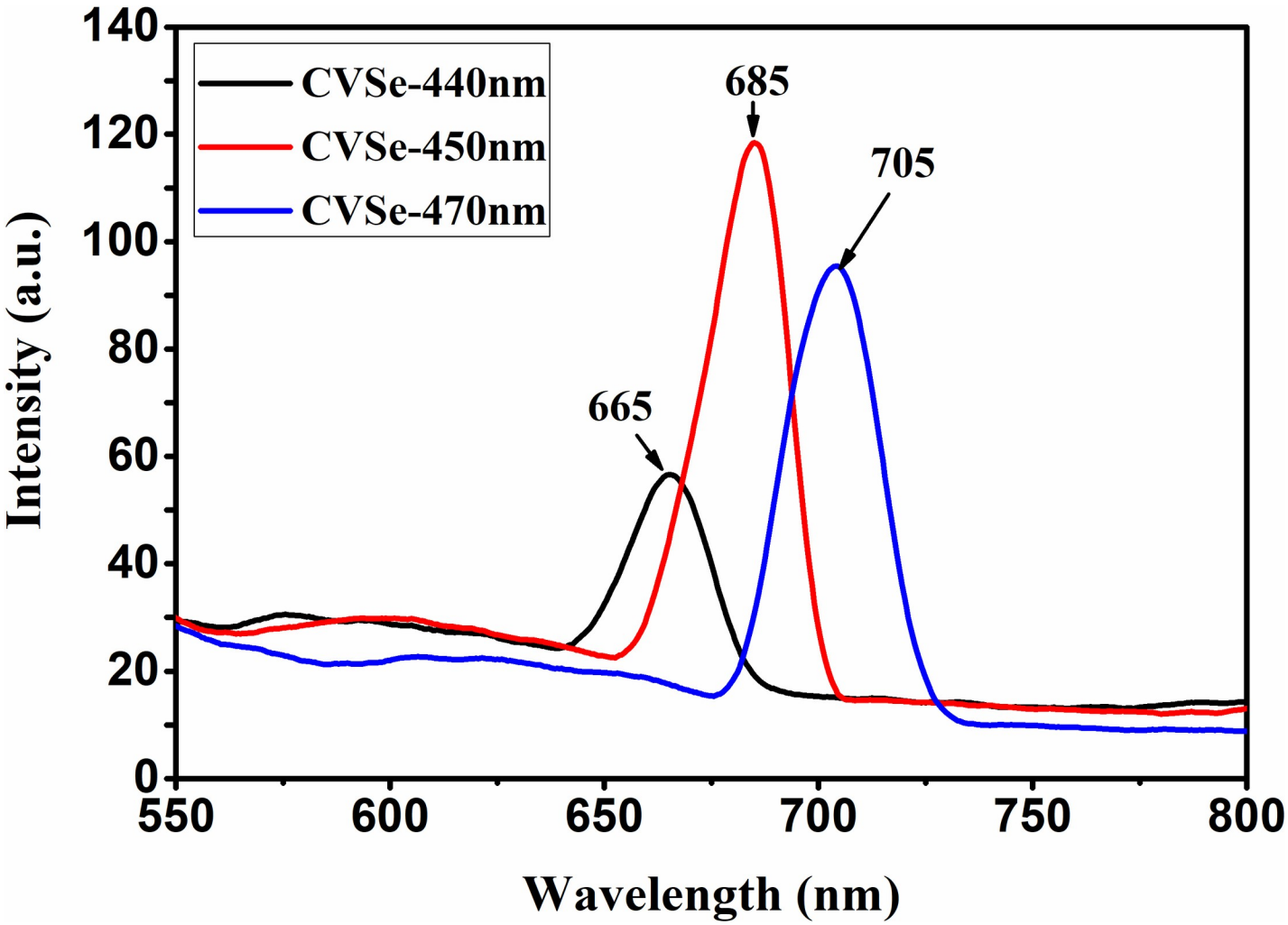

Fig 5. The photoluminescence (PL) spectra of synthesized CVSe NCs using different excitation wavelengths.

https://doi.org/10.1371/journal.pone.0232184.g005

Fig 5 shows the photoluminescence (PL) spectra of synthesized CVSe NCs using different excitation wavelengths. When the CVSe NCs are excited at the wavelength of 440 nm, the emission maximum locates at 665 nm. However, when increasing the excitation wavelength to 450 nm the emission maximum consequently shifts to 685 nm. As the peak of 685 nm possesses the highest intensity, thus, we prefer the 450 nm as the excitation wavelength of CVSe NCs. In other words, the optical bandgap of CVSe NCs is around 1.81 eV, in good agreement with the prediction from the above UV-Vis-NIR spectrum. Overall, the PL peak of CVSe NCs steadily shifts to the red region with the red-shift of the excitation wavelength. Possible explanation for this excitation-dependent PL phenomenon relates to the size distribution of CVSe NCs and the distribution of different emissive sites on the NCs. [30–33]

To study the photoelectrochemical response of CVSe NCs we set up a three-electrode photoelectrochemical cell, as shown in Fig 6A. The current-voltage (J-V) curve of the fabricated CVSe thin film was investigated using a PINE research potentiostat by chopping the LED light with 10 seconds on and 10 seconds off, as shown in Fig 6B, where the current change progressively decreases along with the voltage bias towards positive, implying the p-type semiconductor characteristics of CVSe NCs. When the incident light illuminates the

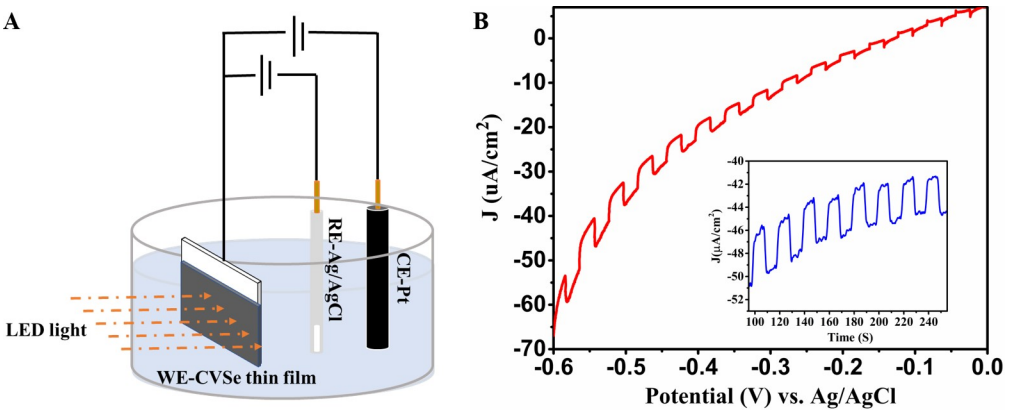

Fig 6. (A) Scheme of CVSe based three-electrodes photoelectrochemical cell. (B) Current-voltage (JV) curve of the CVSe thin film in KCl aqueous solution; insert graph is photocurrent response of the CVSe thin film in KCl aqueous solution at -550 mV.

https://doi.org/10.1371/journal.pone.0232184.g006

surface of the CVSe film, it generates electrons and holes. The photogenerated electrons transport to the interface of electrode/electrolyte and then reduce the H^+ in the electrolyte to H_2, whereas, the photogenerated holes transfer to the counter electrode through the external circuits and promotes the oxidation reaction ($2Cl^- \rightarrow Cl_2$ *or* $\frac{1}{2}H_2O \rightarrow H^+ + O_2$). [34] In the chronoamperometry experiment, as shown in the inset diagram of **Fig 6B**, the photocurrent response of CVSe thin film in KCl aqueous solution was evaluated at -550 mV through several 10 seconds light on–off cycles where the CVSe thin film shows a photocurrent of ~ 4 μA/cm^2 and high stability of the photocurrent. A potential reason for the low photocurrent of CVSe film could be the insufficient continuity of the CVSe thin film used. Both factors could affect the photoelectrochemical behavior of CVSe NCs; the film defects influences the transport of charge carriers. [35] Noteworthy, the CVSe film showed high stability in KCl aqueous solution, as it exhibits the correct Raman spectrum and active photocurrent response after being kept in the aqueous solution for one week. (**S4 Fig** and **S5 Fig**).

To demonstrate the stable photoelectrochemical behavior of CVSe NCs, we measured the photocurrent response of three different CVSe thin films. All of the three different CVSe films display active photoelectrochemical behavior, as shown in **S6 Fig**. Thus, although the generated photocurrent is small, it is non-negligible and it is reproducible.

Conclusions

We reported a facile solution-phase synthetic process to prepare the sulvanite-structured semiconductor Cu_3VSe_4 nanocrystals with cubic shape and an average particle size of about 25 nm. The UV-Vis-NIR spectra shows three main absorption bands in the UV-Vis range, indicating it possesses intermediate band. Thus, when compared to other solution-processed PV materials, CVSe NCs have an intermediate band, which is predicted to be able to absorb energies below the bandgap energy through two optical transitions from the valence to the intermediate band and from intermediate to the conduction band, resulting in enhanced conversion efficiency. Additionally, CVSe NCs possess relatively earth-abundant elements including copper, vanadium, and selenium. Interestingly, the PL peaks shift to red side when increasing the excitation wavelength, which could be attributed to a slight size distribution. The obtained Cu_3VSe_4 nanocrystals were subjected to a ligand exchange process with Na_2S and then coated on FTO substrates to fabricate CVSe-FTO thin films. The CVSe thin films exhibited p-type

photocurrents and photocurrents of ~ 4 μA/cm^2 were recorded when immersing the film in a KCl aqueous electrolyte.

The photocurrent is stable and reproducible, suggesting that by optimizing both particles surface ligands, film fabrication techniques, and using an adequate device architecture, CVSe could become a significant player in solar photovoltaic applications.

Supporting information

S1 Fig. XRD pattern of CVSe NCs annealed for 1 minute (blue) and 5 minutes (purple).
(TIF)

S2 Fig. XRD pattern of as-synthesized CVSe NCs (bottom) and the CVSe NCs after ligand exchange (top).
(TIF)

S3 Fig. Raman spectra of as-synthesized CVSe NCs (bottom) and the CVSe NCs after ligand exchange (top).
(TIF)

S4 Fig. Raman spectra of the CVSe thin film. Dark line is the Raman spectrum of fresh CVSe thin film; Red graph is the Raman spectrum of the CVSe film that was kept in KCl aqueous solution for 1 week.
(TIF)

S5 Fig. Current-voltage (JV) curve of the CVSe thin film in KCl aqueous solution. Dark line is the JV curve of fresh CVSe thin film; Red line is the JV curve of CVSe film kept in KCl aqueous solution for 1 week.
(TIF)

S6 Fig. Photocurrent response of three different CVSe thin films.
(TIF)

Acknowledgments

The authors are very grateful to Prof. Zhiqun Lin and his group at Georgia Institute of Technology for access to PL instrumentation.

Also, the authors would like to thank Dr. Federico Rosei at the Institute National de la Recherche Scientifique (INRS), Canada for access to his research facilities.

Author Contributions

Conceptualization: Mimi Liu, Cheng-Yu Lai, Daniela R. Radu.

Formal analysis: Cheng-Yu Lai.

Funding acquisition: Cheng-Yu Lai, Daniela R. Radu.

Methodology: Mimi Liu, Gurpreet Singh Selopal.

Project administration: Cheng-Yu Lai.

Supervision: Cheng-Yu Lai, Daniela R. Radu.

Writing – original draft: Mimi Liu, Cheng-Yu Lai, Daniela R. Radu.

Writing – review & editing: Mimi Liu, Cheng-Yu Lai, Gurpreet Singh Selopal, Daniela R. Radu.

References

1. Ali A, Jahan N, Islam AKM. Sulvanite Compounds Cu3TMS4 (TM = V, Nb and Ta): Elastic, Electronic, Optical and Thermal Properties using Firstprinciples Method. Journal of Scientific Research. 2014; 6:407–19. https://doi.org/10.3329/jsr.v6i3.19191
2. Hong AJ, Yuan CL, Gu G, Liu JM. Novel p-type thermoelectric materials Cu3MCh4 (M = V, Nb, Ta; Ch = Se, Te): high band-degeneracy. Journal of Materials Chemistry A. 2017; 5(20):9785–92. https://doi.org/10.1039/C7TA02178J
3. Kehoe AB, Scanlon DO, Watson GW. The electronic structure of sulvanite structured semiconductors Cu3MCh4 (M = V, Nb, Ta; Ch = S, Se, Te): prospects for optoelectronic applications. Journal of Materials Chemistry C. 2015; 3(47):12236–44. https://doi.org/10.1039/C5TC02760H
4. Kehoe AB, Scanlon DO, Watson GW. Modelling potential photovoltaic absorbers Cu3MCh4 (M = V, Nb, Ta; Ch = S, Se, Te) using density functional theory. Journal of Physics Condensed Matter. 2016; 28 (17). https://doi.org/10.1088/0953-8984/28/17/175801 PMID: 27033972
5. Ntholeng N, Mojela B, Gqoba S, Airo M, Govindraju S, Moloto MJ, et al. Colloidal synthesis of pure CuInTe2 crystallites based on the HSAB theory. New Journal of Chemistry. 2016; 40(12):10259–66. https://doi.org/10.1039/C6NJ02108E
6. van Embden J, Chesman ASR, Jasieniak JJ. The Heat-Up Synthesis of Colloidal Nanocrystals. Chemistry of Materials. 2015; 27(7):2246–85. https://doi.org/10.1021/cm5028964
7. Ikeda S, Aono N, Iwase A, Kobayashi H, Kudo A. Cu3MS4 (M = V, Nb, Ta) and its Solid Solutions with Sulvanite Structure for Photocatalytic and Photoelectrochemical H2 Evolution under Visible-Light Irradiation. ChemSusChem. 2019; 12(9):1977–83. https://doi.org/10.1002/cssc.201802702 PMID: 30666792
8. Todorov T, Gunawan O, Chey SJ, de Monsabert TG, Prabhakar A, Mitzi DB. Progress towards marketable earth-abundant chalcogenide solar cells. Thin Solid Films. 2011; 519(21):7378–81. https://doi.org/10.1016/j.tsf.2010.12.225.
9. Chen C-C, Stone KH, Lai C-Y, Dobson KD, Radu D. Sulvanite (Cu3VS4) nanocrystals for printable thin film photovoltaics. Materials Letters. 2018; 211:179–82. https://doi.org/10.1016/j.matlet.2017.09.063.
10. Mantella V, Ninova S, Saris S, Loiudice A, Aschauer U, Buonsanti R. Synthesis and Size-Dependent Optical Properties of Intermediate Band Gap Cu3VS4 Nanocrystals. Chemistry of Materials. 2019; 31 (2):532–40. https://doi.org/10.1021/acs.chemmater.8b04610
11. Luque A, Martí A, Stanley C. Understanding intermediate-band solar cells. Nature Photonics. 2012; 6:146. https://doi.org/10.1038/nphoton.2012.1
12. Hanna MC, Nozik AJ. Solar conversion efficiency of photovoltaic and photoelectrolysis cells with carrier multiplication absorbers. Journal of Applied Physics. 2006; 100(7):074510. https://doi.org/10.1063/1.2356795
13. Vörös M, Galli G, Zimanyi GT. Colloidal Nanoparticles for Intermediate Band Solar Cells. ACS Nano. 2015; 9(7):6882–90. https://doi.org/10.1021/acsnano.5b00332 PMID: 26042468
14. Huang TJ, Yin X, Tang C, Qi G, Gong H. A low-cost, ligand exchange-free strategy to synthesize large-grained Cu2ZnSnS4 thin-films without a fine-grain underlayer from nanocrystals. Journal of Materials Chemistry A. 2015; 3(34):17788–96. https://doi.org/10.1039/C5TA03640B
15. Nag A, Kovalenko MV, Lee J-S, Liu W, Spokoyny B, Talapin DV. Metal-free Inorganic Ligands for Colloidal Nanocrystals: S2–, HS–, Se2–, HSe–, Te2–, HTe–, TeS32–, OH–, and NH2– as Surface Ligands. Journal of the American Chemical Society. 2011; 133(27):10612–20. https://doi.org/10.1021/ja2029415 PMID: 21682249
16. Talapin DV, Lee J-S, Kovalenko MV, Shevchenko EV. Prospects of Colloidal Nanocrystals for Electronic and Optoelectronic Applications. Chemical Reviews. 2010; 110(1):389–458. https://doi.org/10.1021/cr900137k PMID: 19958036
17. Kim M-w, Joshi B, Yoon H, Ohm TY, Kim K, Al-Deyab SS, et al. Electrosprayed copper hexaoxodivanadate (CuV2O6) and pyrovanadate (Cu2V2O7) photoanodes for efficient solar water splitting. Journal of Alloys and Compounds. 2017; 708:444–50. https://doi.org/10.1016/j.jallcom.2017.02.302.
18. Mohammadnezhad M, Liu M, Selopal GS, Navarro-Pardo F, Wang ZM, Stansfield B, et al. Synthesis of highly efficient Cu2ZnSnSxSe4−x (CZTSSe) nanosheet electrocatalyst for dye-sensitized solar cells. Electrochimica Acta. 2020; 340:135954. https://doi.org/10.1016/j.electacta.2020.135954.
19. Zhang X, Tang Y, Wang Y, Shen L, Gupta A, Bao N. Simple one-pot synthesis of Cu4SnS4 nanoplates and temperature-induced phase transformation mechanism. CrystEngComm. 2020; 22(7):1220–9. https://doi.org/10.1039/C9CE01772K
20. Lindström R, Maurice V, Zanna S, Klein L, Groult H, Perrigaud L, et al. Thin films of vanadium oxide grown on vanadium metal: oxidation conditions to produce V2O5 films for Li-intercalation applications

and characterisation by XPS, AFM, RBS/NRA. Surface and Interface Analysis. 2006; 38(1):6–18. https://doi.org/10.1002/sia.2141

21. Wang W, Jiang J, Ding T, Wang C, Zuo J, Yang Q. Alternative Synthesis of CuFeSe2 Nanocrystals with Magnetic and Photoelectric Properties. ACS Applied Materials & Interfaces. 2015; 7(4):2235–41. https://doi.org/10.1021/am508844w PMID: 25562289

22. Dash S, Kajita T, Yoshino T, Saini NL, Katsufuji T, Mizokawa T. V 2p core-level spectroscopy of V2+/V3 + mixed valence AV10O15 (A = Ba, Sr) and Ba0.9Sr0.1V13O18. Journal of Electron Spectroscopy and Related Phenomena. 2018; 223:11–20. https://doi.org/10.1016/j.elspec.2017.12.002.

23. Laurenti M, Castellino M, Perrone D, Asvarov A, Canavese G, Chiolerio A. Lead-free piezoelectrics: V (3+) to V(5+) ion conversion promoting the performances of V-doped Zinc Oxide. Sci Rep. 2017; 7:41957–. https://doi.org/10.1038/srep41957 PMID: 28165040.

24. Wang F, Wang Z, Shifa TA, Wen Y, Wang F, Zhan X, et al. Two-Dimensional Non-Layered Materials: Synthesis, Properties and Applications. Advanced Functional Materials. 2017; 27(19):1603254. https://doi.org/10.1002/adfm.201603254

25. Bernede JC, Hamdadou N, Khelil A. X-ray photoelectron spectroscopy study of CuFeSe2 thin films. Journal of Electron Spectroscopy and Related Phenomena. 2004; 141(1):61–6. https://doi.org/10.1016/j.elspec.2004.07.003.

26. Chen G, Yuan C, Liu J, Deng Y, Jiang G, Liu W, et al. Low cost preparation of Cu2ZnSnS4 and Cu2ZnSn(SxSe1−x)4 from binary sulfide nanoparticles for solar cell application. Journal of Power Sources. 2014; 262:201–6. https://doi.org/10.1016/j.jpowsour.2014.03.075.

27. Zhou X, Gao P, Sun S, Bao D, Wang Y, Li X, et al. Amorphous, Crystalline and Crystalline/Amorphous Selenium Nanowires and Their Different (De)Lithiation Mechanisms. Chemistry of Materials. 2015; 27 (19):6730–6. https://doi.org/10.1021/acs.chemmater.5b02753

28. Bastola E, Bhandari KP, Subedi I, Podraza NJ, Ellingson RJ. Structural, optical, and hole transport properties of earth-abundant chalcopyrite (CuFeS2) nanocrystals. MRS Communications. 2018; 8 (3):970–8. Epub 2018/07/04. https://doi.org/10.1557/mrc.2018.117

29. Oguchi T, Sato K, Teranishi T. Optical Reflectivity Spectrum of a CuFeS2 Single Crystal. Journal of the Physical Society of Japan. 1980; 48(1):123–8. https://doi.org/10.1143/JPSJ.48.123

30. Pan D, Zhang J, Li Z, Wu C, Yan X, Wu M. Observation of pH-, solvent-, spin-, and excitation-dependent blue photoluminescence from carbon nanoparticles. Chem Commun (Camb). 2010; 46(21):3681–3. https://doi.org/10.1039/c000114g PMID: 20396809.

31. Sun Y-P, Zhou B, Lin Y, Wang W, Fernando KAS, Pathak P, et al. Quantum-Sized Carbon Dots for Bright and Colorful Photoluminescence. Journal of the American Chemical Society. 2006; 128 (24):7756–7. https://doi.org/10.1021/ja062677d PMID: 16771487

32. Wang H, Sun C, Chen X, Zhang Y, Colvin VL, Rice Q, et al. Excitation wavelength independent visible color emission of carbon dots. Nanoscale. 2017; 9(5):1909–15. https://doi.org/10.1039/c6nr09200d PMID: 28094404

33. Zhou J, Sheng Z, Han H, Zou M, Li C. Facile synthesis of fluorescent carbon dots using watermelon peel as a carbon source. Materials Letters. 2012; 66(1):222–4. https://doi.org/10.1016/j.matlet.2011.08.081.

34. Wei X, Qiu Y, Duan W, Liu Z. Cathodic and anodic photocurrents generation from melem and its derivatives. RSC Advances. 2015; 5(34):26675–9. https://doi.org/10.1039/C5RA02816G

35. Valaski R, Ayoub S, Micaroni L, Hümmelgen IA. Influence of film thickness on charge transport of electrodeposited polypyrrole thin films. Thin Solid Films. 2002; 415(1):206–10. https://doi.org/10.1016/S0040-6090(02)00553-9.